Journal of
Marine Science and Engineering

MDPI

Article

Acoustic Source Characterization of Marine Propulsors

Jukka Tanttari and Antti Hynninen *

VTT Technical Research Centre of Finland Ltd., Tekniikantie 21, 02150 Espoo, Finland; jukka.tanttari@vtt.fi
* Correspondence: antti.hynninen@vtt.fi

Abstract: Marine propulsors represent one of the most important contributors among anthropogenic sounds radiated into water. Blade based propulsors, e.g., propellers, generate tones at the blade passing frequency and its harmonics, especially in cavitating conditions. In addition to hydrodynamic noise, pressure fluctuations cause vibrations in ship hull leading to mechanical noise. For noise prediction purposes, it is highly beneficial to characterize the noise sources as simplified, complex valued arrays having information on source positions, source strengths and phases. In this paper, procedure to characterize marine propulsors as acoustic sources with inverse method is introduced. First, the numerical model with complete hydro-acoustic sources is investigated. Second, a source model composed of sensible number and distribution of elementary ("equivalent") compact sources is specified. Then selected responses are used as input in source characterization with inverse method. Finally, the model with equivalent sources is solved and the results are validated by comparison against the results from the complete simulation model. The introduced acoustic source characterization procedure of marine propulsors is applicable also for the responses determined experimentally, e.g., in a cavitation tunnel when the pressure transducer array is determined appropriately.

Keywords: acoustic source characterization; marine propulsor noise; equivalent source method; inverse method; cavitation; cavitation tunnel experiments

check for updates

Citation: Tanttari, J.; Hynninen, A. Acoustic Source Characterization of Marine Propulsors. *J. Mar. Sci. Eng.* **2022**, *10*, 1273. https://doi.org/10.3390/jmse10091273

Academic Editors: Mehmet Atlar and Savas Sezen

Received: 3 August 2022
Accepted: 6 September 2022
Published: 9 September 2022

Publisher's Note: MDPI stays neutral with regard to jurisdictional claims in published maps and institutional affiliations.

1. Introduction

Sound is vibration that propagates as an acoustic wave, through a transmission medium such as gas, liquid or solid. Noise is unwanted sound that is considered unpleasant, loud, or disruptive to hearing. Thus, sound and noise are indistinguishable from the physical point of view. Underwater noise can be considered as unwanted sound emitted by a source, transmitted to an underwater receiver where it is immitted. It should be noted that "pollution" in marine context means introduction of substances or energy, including underwater noise, into the environment [1,2]. Emission of a noise source is described using two quantities, sound power and directivity. Directivity is a measure of variation of sound radiation with direction, often stated as a function of angular position. Immission is usually quantified as sound pressure level at certain location. It depends on transfer path, i.e., acoustic environment and the positions of the source and the receiver.

1.1. Underwater Radiated Noise

Underwater radiated noise (URN) is a subject of increasing importance due to its harmful impact on the marine environment, especially in regions where ships and marine life coexist. Increased shipping rates correlate with observed elevation in underwater noise levels. The underwater noise pollution is a significant threat to aquatic ecosystems, and anthropogenic sound is noted as one of the most detrimental types of pollution [3]. Limiting acoustic emissions from shipping is at present a major concern, and abatement of noise pollution also from shipping is foreseen in the near future either via technological advancements or policy commitments [4]. National as well as international rules and guidelines are inclining toward more strict limitations regarding the allowable underwater noise levels [5–8].

A ship is a complex system consisting of large number of components, whose acoustic behaviour may be relatively unknown and depends on different and complicated physical phenomena. One way to categorize the noise sources of a ship is separation into machinery noise and hydrodynamic noise [9]. The excitations to the structural vibrations of the hull are the machines such as main engines, gears, generators, pumps, and electric machines. Hydrodynamic noise covers the blade rate noise of the rotating propulsor, flow noise due to turbulence and vortices, propulsor singing due to resonances as well as cavitation at the propulsor and at the other water connected structures. Periodic fluctuations of the cavitation volumes generate tones at the blade passing frequency and its harmonics. Randomly occurring collapses of the cavitation voids generate broadband noise. It is worth noting, that hydrodynamic noise and machinery noise are interconnected due to cavitation excitation of the structural vibrations. Due to the interconnection of the underwater radiated noise phenomena, it is impossible to distinguish the root causes of the noise from a limited number of response signals.

1.2. Model-Scale Tests

Model-scale tests in a cavitation tunnel are commonly used to predict the radiated noise from full-scale propulsors. Noise measurements are usually performed using one or more hydrophones mounted in the test facility where the propulsor is tested. First, the effect of the background noise is eliminated. Then the propagation loss due to geometrical spreading and sound attenuation are considered using somehow determined corrections functions. Finally, the underwater radiated noise of a full-scale propulsor is predicted using scaling laws. A compendium of tunnel- and hydrophone installations is available in [10–13], for example. However, cavitation tunnel environment also alters the fundamental sound emission of the propulsor compared to emission of the same propulsor in free-field conditions. This, together with the lack of adequate standards, makes the experimental noise source characterization with the present methods highly inaccurate. See, e.g., investigations on different tunnel facilities in [14,15].

The ratio of sound pressure responses in different points in tunnel environment differs from that in free space or another environment. Thus, any effort to "transfer" results from tunnel to another environment using ratios of some field point pressures (sometimes these ratios are misleadingly named "transfer functions") does not work. A method separating environment-independent source properties, field responses and relevant transfer functions explicitly from each other is needed.

1.3. Numerical Methods

Nowadays, numerical methods are widely used for propulsor performance estimations. Lot of work has been conducted for their verification and validation, see, e.g., [16–18]. Numerical methods can also provide understanding to the generation and propagation of the underwater radiated noise. In principle, the most general approach for numerical acoustic simulations concerns direct numerical simulation (DNS) of the governing flow conservation equations for mass, momentum, and energy, since the numerical flow solution includes both sound generation and its propagation. Unfortunately, DNS is computationally extremely expensive and generally limited to problems with low Reynolds numbers. On the other hand, acoustic analogies may be utilized for the assessment of flow-induced noise based on an a priori flow solution from computation fluid dynamics (CFD). Acoustic analogies are investigated thoroughly in [19]. The propeller-induced free field noise via utilization of the Ffowcs Williams–Hawkings acoustic analogy to the CFD results has been widely studied, see, e.g., [20–22]. In practice, the assumption of a free field is not valid. The propulsor interacts acoustically with its surroundings, e.g., with the cavitation tunnel or with the ship structure, sea bed and sea surface. Due to huge amount of computational resources required in DNS or CFD, these simulations cannot be used as such when rapid noise estimations are required, in digital twins for example.

In the hybrid computational hydro-acoustic (CHA) approach, which is also applied here, the numerical flow solution from CFD is required only near the noise sources and acoustic solution is used for modelling the surrounding environment [16]. Acoustic finite element method (FEM) or boundary element method (BEM) are then used for modelling the surrounding environment.

1.4. Acoustic Source Characterization

In the acoustic source characterization, the aim is not to obtain an accurate representation of source mechanisms but represent the source with elementary components that yield to similar net effect on the surroundings. For noise prediction purposes, it is highly beneficial to characterize the noise sources as simplified, complex valued arrays having information on source positions, source strengths and phases.

The methods applied appear in literature under many different names, like "fictitious source method", "substitute source method" and "equivalent source method", to mention a few. However, irrespective of the application, the underlying theoretical idea is the same: to use a number infinitely small elementary sources to replace the "real" source, see, e.g., [23–35]. The strengths of the sources are found by matching the actual radiated sound field with the modelled sound field in several points or as an average on a given surface, see Figure 1. Here, the term "inverse" or "inverse method" refers to the mathematical technique of using the inverse of the transfer matrix to solve the source strengths. The term "equivalent source" or "equivalent source method" refers to the aim of determining source strengths producing sound radiation equivalent with the actual source distribution.

In an equivalent source model, the "real" source is modelled using M ideal, elementary sources (usually monopoles) distributed over the radiating surface of the source. The idea is to define a limited number of sources, which produce same ("equivalent") response than the real source distribution or -mechanism. The acoustic field generated by the sources is quantified using N field points, usually placed relatively near the source.

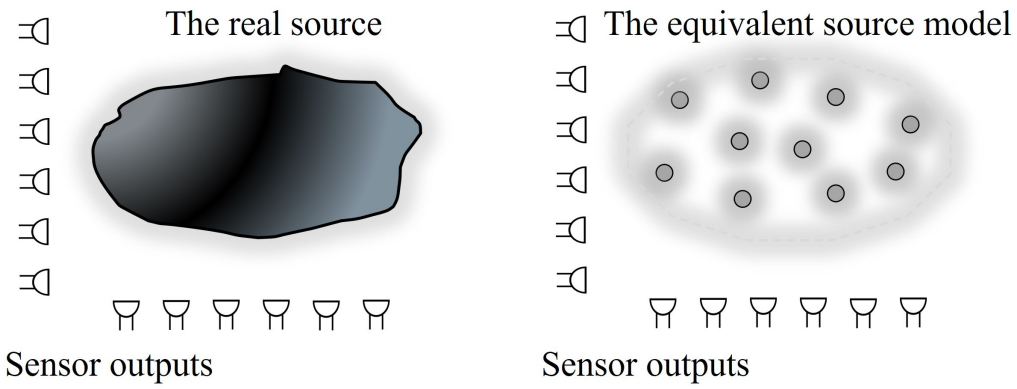

Figure 1. The equivalent source method in nutshell. In this example, M = 10 and N = 12.

1.5. The Novelty of the Work

The novelty of the work is rigorous acoustic source characterization of a propeller in a cavitation tunnel. A combination of numerical hydro-acoustic and acoustic simulations followed by matrix calculations of the equivalent source method is used. The process yields the propeller source model uncoupled from the acoustic environment. To authors' knowledge this kind of procedure and results are not previously published for a propeller source in a cavitation tunnel.

2. Methods

In this work, hybrid CHA approach is used for generating the input data. First, the noise source terms are derived from CFD results to acoustic FEM simulations. Then acoustic BEM simulations and matrix calculations are used for determination of equivalent source

strengths. The overall flowchart of the calculations leading to equivalent source model is in Figure 2.

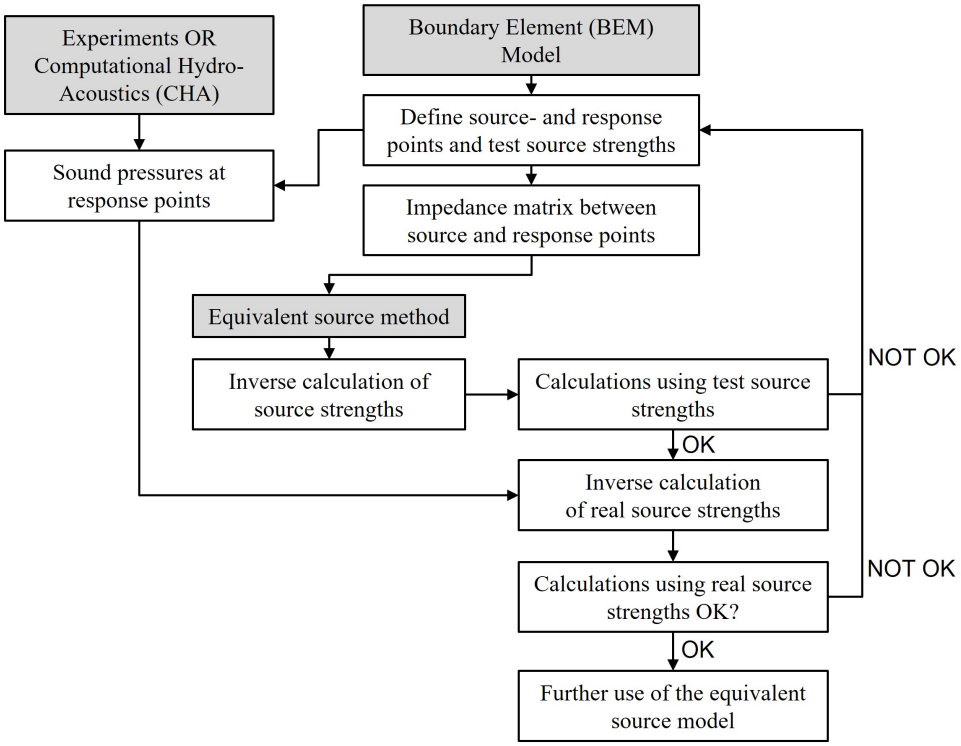

Figure 2. Flowchart of the calculations leading to equivalent source model.

2.1. Complete CHA Simulation Model

CFD is commonly used to simulate cavitation and the turbulent flow around the propulsor. Using the excitations from CFD, the hydrodynamic noise as well as mechanical noise can be then simulated using acoustic FEM, see [16]. Using Lighthill analogy, the wave equation is

$$-\omega^2\rho - c_0^2\Delta\rho = \frac{\partial^2 T_{ij}}{\partial x_i \partial x_j}, \tag{1}$$

where ρ is density, c_0 is the speed of sound in the medium, ω is the angular velocity and T_{ij} is the Lighthill tensor. Using the Gauss theorem, FEM formulation of the wave equation is obtained

$$\omega^2 \int_\Omega N\rho \mathrm{d}\Omega - \int_\Omega \frac{\partial N}{\partial x_i} c_0^2 \frac{\partial \rho}{\partial x_i} \mathrm{d}\Omega = i\omega \int_\Gamma N\rho v_i n_i \mathrm{d}\Gamma + \int_\Omega \frac{\partial N}{\partial x_i} \frac{\partial T_{ij}}{\partial x_i} \mathrm{d}\Omega, \tag{2}$$

where Ω is the volume and Γ is the surface of the boundary enclosing the propulsor, N are the shape functions and v is velocity. Using this formulation, the volume and surface source term influences can be evaluated separately.

It should be noted that in this study the complete simulation model is used to produce input and comparison data for the equivalent source model. That is, sound pressure responses at selected field points are needed. This data can be derived experimentally as well. Here, only the acoustic sources inside the conformal surface are considered in the input data simulations. Estimating the accuracy of the complete simulation model with volume and surface sources requires extensive computing resources and is therefore beyond this study.

In free space far field conditions, acoustic waves spread radially from the source. The distribution of sound pressure at certain distance but different angles depend on the directivity. However, the local wave front approaches asymptotically a plane wave and

spreading of sound pressure in certain direction follows the $1/r$-law. Conditions in a tunnel are completely different [36]. The nearby surfaces effect the radiation of sound from a source. If the surface is idealized as rigid, planar, and infinite, the original boundary-value problem of source plus wall can be replaced with two sources, i.e., original and image source. For a case with more than one walls, also the images of the images must be considered. For a source in an infinite long rectangular duct, there is a twofold infinity of image sources, all lying in a plane transverse to the duct. The propagation is limited to the axial direction by the tunnel walls and up to high frequencies, as tunnel cross-section dimensions are small compared to the wavelength and walls are at the near field of the source. See, e.g., [37] for details. In this study, the acoustic behaviour of the propulsor is investigated in a tunnel and in free field.

The idea in inverse source fits is to start from the response, for example the induced pressure field. Then, the task is to decide the form of the equivalent source system and fit source strengths as well as source phases to produce the same response as the original.

2.2. Inverse Source Fit

Typically, the system is overdetermined; more responses than sources: $N \geq M$. The vector p of sound pressure in the field points equals to product of transfer matrix H and the vector of source volume velocities, q. Definition of monopole source strength as volume velocity, see, e.g., [38] All quantities are complex:

$$p = Hq. \tag{3}$$

The task is to determine the equivalent source vector "inversely", i.e., utilizing the known pressures induced by the real source in the field points and the known (calculated using BEM) transfer matrix H. However, the process is not straightforward for an overdetermined system. The matrix H is not a square matrix and hence it is not directly invertible. The workaround is to use the pseudo-inverse H^+ of the transfer matrix. A method for obtaining the H^+ is the singular value decomposition (SVD). The transfer matrix is composed of matrices U ($N \times N$, left singular vectors of responses), Σ ($N \times M$, a diagonal matrix of singular values) and V ($M \times M$, right singular vectors of sources):

$$H = U\Sigma V^H, \tag{4}$$

where the superscript H indicates the Hermitian transpose (conjugate transpose). Now the pseudo-inverse H^+ of H is formed according to

$$H^+ = V\Sigma^+ U^H \tag{5}$$

where Σ^+ is the pseudo-inverse of Σ. The non-zero elements of the diagonal ($M \times N$) matrix Σ^+ are reciprocals of the non-zero singular values in Σ. The source vector is calculated from

$$q = H^+\tilde{p} = V\Sigma^+ U^H\tilde{p}, \tag{6}$$

where $\tilde{p}$ contains pressures calculated or measured at sensor points. It contains inevitable measurement and calculation errors e and, hence, differs vector of "precise" pressures p according to

$$p = \tilde{p} + e. \tag{7}$$

Note that only in simplest cases, like free field in unbounded 3D-space or half-space, the transfer functions have analytic solutions. For general acoustic environment they must be measured or calculated numerically.

2.3. Solution Sensitivity of Inverse Source Fit

It is well known that the transfer matrix to be inverted tends to be ill-conditioned, especially as the number of equivalent sources is increased. Under the unavoidable pres-

ence of noise, the quantification of the equivalent sources is crucially dependent on the conditioning of the problem. The sensitivity of solution for source strengths q to small errors in the transfer matrix H or responses $\tilde{p}$ is determined by the condition number $\kappa(H)$ of the transfer matrix to be inverted. Definition of the condition number is

$$\kappa(H) = \|H\|\|H^{-1}\| \tag{8}$$

or, when pseudo-inverse of H is used,

$$\kappa(H) = \|H\|\|H^{+}\| \tag{9}$$

where $\|H\|$ denotes the 2-norm of the matrix. The 2-norm of H is equal to the largest singular value (σ_{Max}) of H. The 2-norm of H^{+} is equal to $1/\sigma_n$, where σ_n is the smallest non-zero singular value of H. If small deviations δp of p produce small deviations δq in the solution of q, then

$$H(q + \delta q) = (p + \delta p) \tag{10}$$

Utilizing properties of matrix 2-norms we may write Nelson & Yoon, 2000 [23]

$$\frac{\|\delta q\|}{\|q\|} \leq \|H\|\|H^{+}\| \frac{\|\delta p\|}{\|p\|} \tag{11}$$

and, finally,

$$\frac{\|\delta q\|}{\|q\|} \leq \kappa(H) \frac{\|\delta p\|}{\|p\|} \tag{12}$$

Note that Equation (12) does not give exact values for the deviation (perturbation) of the solution, but merely an upper limit. Hence, the condition number serves as a risk analysis indicator. Although it is, in general, not straightforward to judge the boundary between "small" and "large" condition numbers, the condition numbers can be said to be small enough, when they are below about 10^3 [24,27]. Then the least-squares method used in pseudo-inverse can provide a satisfactory reconstruction, without using special regularization methods [24].

It is also probable, that also the condition number increases, when the number of equivalent sources increases. And vice versa: in the limiting case of one source and one response, the condition number is 1. This is because, in case of linear system, driven with only one source, the relative deviation in the response are equal to the relative deviation in the source to be determined.

2.4. The Process for an Equivalent Source Model

Determination on source strengths for the equivalent source model is as follows.

1. A plausible number and distribution of sources is defined;
2. The number and locations of sensor points is chosen;
3. Transfer matrix from source points and sensor points is determined. Sources placed in source points are activated one at the time, yielding response/source transfer vectors. This is repeated for all source points yielding the full transfer matrix and then its pseudo-inverse. In this work, BEM is used throughout in "forward" acoustic calculations using Equation (3) from sources to sensors. Matrix calculations, Equations (4)–(6) are most conveniently conducted with MATLAB or similar;
4. The equivalent source model is tested using pressures calculated with given (known) source vector. The source vector is determined using the inverse method and compared to the given source vector. Corrections for sensor numbers, locations, etc., are made as needed and the test repeated until the accuracy of inversely determined source vector with respect to the given source vector is sufficient;
5. The actual measured or calculated pressure vector is multiplied with the transfer matrix pseudo-inverse. This step yields the equivalent source vector;

6. The equivalent source vector is tested in re-producing the measured or calculated pressures. Corrections are made as needed;
7. The source model is transferred and used in a different environment as a equivalent source model.

3. Test Case

A propeller by Schiffbau-Versuchsanstalt Potsdam GmbH (SVA Potsdam) shown in Figure 3 was selected as a test case. The Potsdam Propeller Test Case (PPTC) introduced in [39] is intended to offer the possibility to test and validate calculation methods. Different data (geometries, reports and videos) related to propeller flow is freely available in the SVA Potsdam website [40]. Here, the CFD simulation data of the cavitating propeller in uniform homogeneous inflow condition is taken as the input for the acoustic FEM simulations. The CFD simulations were conducted earlier in [16]. In the CFD simulation data used here, $k-\epsilon$ turbulence model was used. Rotating speed of the five bladed propeller is 1200 rpm, i.e., blade passing frequency (BPF) is 100 Hz. The propeller is operating in push configuration. In this study, the simulation data of the operation point two (advance coefficient $J = 1.3$, cavitation number $\sigma_n = 1.424$) in [39] is used. At that operating point, tip vortex and root cavitation at the suction and pressure side appear [41]. More details on the CFD simulation and cavitation modelling can be found from [16,17].

Figure 3. (**left**) The Potsdam Propeller Test Case (PPTC) without hub. (**right**) The conformal surface enclosing the propeller and hub. Diameter of the propeller is 250 mm.

First, the acoustic behaviour of the propeller in a cavitation tunnel was simulated. Acoustic FEM mesh is created for the fluid, i.e., tunnel volume minus the volume enclosed by the conformal surface. Acoustic FEM mesh of the fluid is shown in Figure 4. The mesh consists of approximately 800,000 quadratic tetrahedron elements. More than six elements per the shortest wave length are used, i.e., the model is clearly suitable for up to 3000 Hz. Ends of the cavitation tunnel are modelled as semi-infinite, i.e., reflection free terminations. Conformal surface enclosing the propeller blades and propeller hub is created for the acoustic source data extraction from CFD results and for the creation of the Lighthill's surface sources to the acoustic mesh. The conformal surface is shown in Figure 3.

In addition to the tunnel model, the acoustic behaviour of the PPTC in free field was simulated. The free field model consists of the blue and red parts shown in Figure 4 and from the approximately spherical free field volume model which radius adapts to the simulated frequency range. Note that in this study, only the Lighthill's surface sources are considered, i.e., only the blue part is relevant here. The influence of the Lighthill's volume sources in the red part will be investigated in the future. Free field acoustic FEM model has up to 2.5 M degrees of freedom.

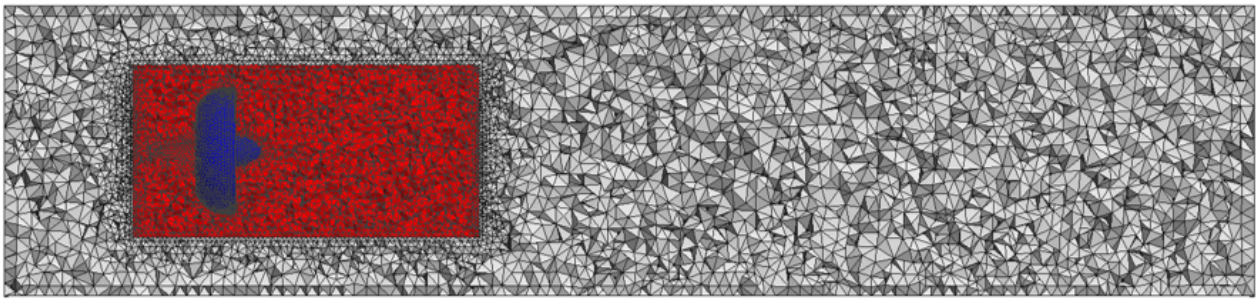

Figure 4. Cut view of the acoustic FEM model of the PPTC in a cavitation tunnel. Lighthill's surface sources are derived from the CFD results and mapped to the conformal surface shown as blue. In addition, Lighthill's volume sources can be mapped to the cylindrical volume shown as red.

4. CHA Simulation Results

The acoustic field was solved from 20 Hz to 3000 Hz with steps of 20 Hz in the cavitation tunnel and in free field using FEM. Acoustic excitations generated from the CFD results create rotating pressure fields near the propeller. Example of the acoustic pressure isosurfaces due to excitations on the conformal surface at 100 Hz is shown at left in Figure 5. The response points at the tunnel wall for the inverse source fit model are shown at right in Figure 5. The response plane for inverse source fitting is located 200 mm downstream from the centre of the propeller.

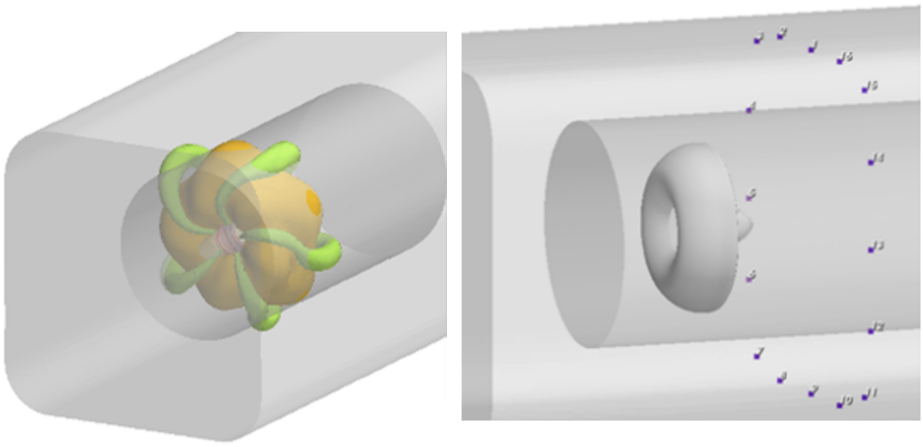

Figure 5. An example of the acoustic pressure isosurfaces due to excitations at 100 Hz on the propeller conformal surface (**left**). The response points at the tunnel wall for the inverse source fit (**right**).

Sound powers of the PPTC in cavitation tunnel and in free field due to surface excitations is shown in Figure 6. Note that the reference value for the sound power is $L_{w,ref} = p_{ref}^2/(\rho c)$, where pressure reference, density and speed of sound in water are $p_{ref} = 1$ µPa, $\rho = 1000$ kg/m^3 and $c = 1448.9$ m/s, respectively. In the figure, also the calculated tunnel effect and the theoretical sound power correction for an acoustic monopole are drawn. The theoretical sound power correction is derived in detail by Pierce [37]. Sound pressure maps at 100 Hz for the propeller in free field and in a cavitation tunnel are shown in Figure 7.

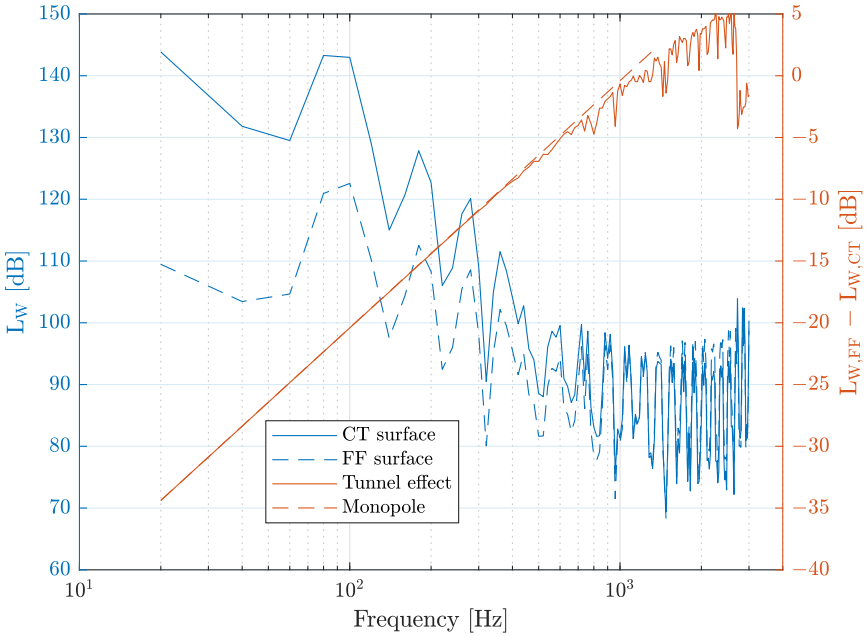

Figure 6. Sound powers of the PPTC in cavitation tunnel (CT) and in free field (FF) due to surface excitations. Also, the calculated tunnel effect and the theoretical sound power correction for an acoustic monopole are drawn.

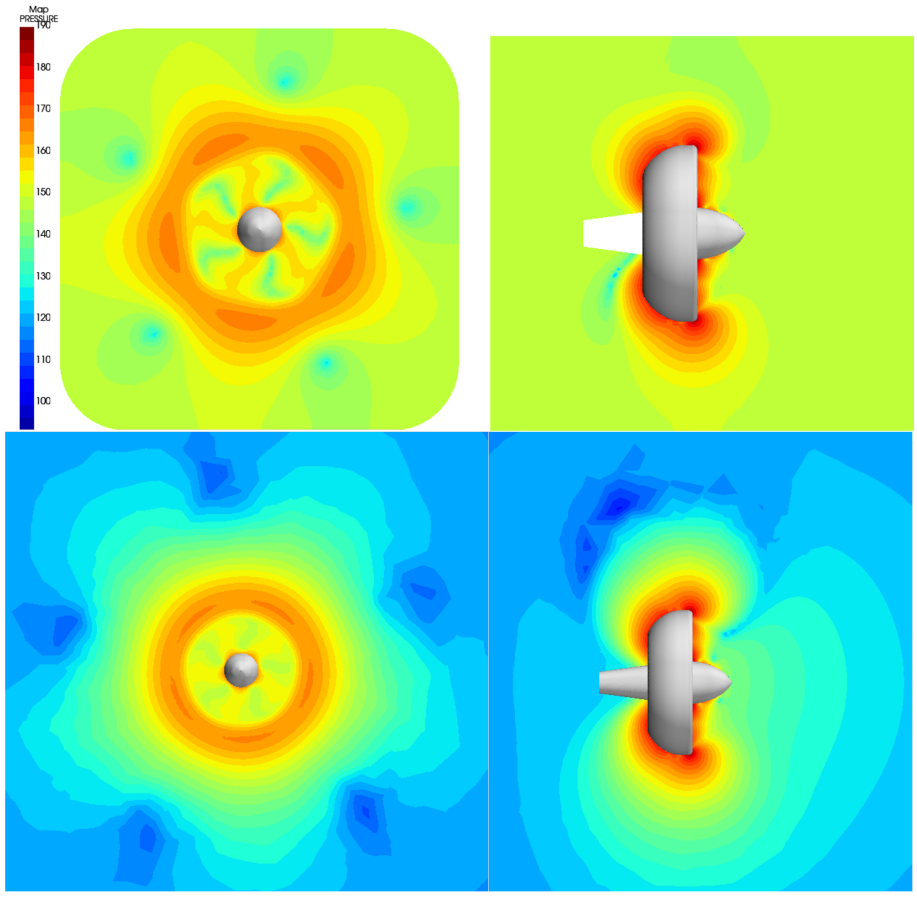

Figure 7. Sound pressure maps at 100 Hz. Propeller in a cavitation tunnel (**top**) and in free field (**bottom**).

5. The Equivalent Source Model

The challenge was to choose optimal number of sources and sensors as well as their spatial distribution. See, e.g., [23–25,27,31]. In this work, the arrangement used by Kim and Nelson [25] for a ducted fan, was used as a paragon. Kim and Nelson used 7 or 9 monopole sources and up to 48 sensors.

The final equivalent source model of the PPTC propeller consists of five monopoles (same as the number of blades) in a ring form (Figure 8). The diameter of the monopole ring is 0.7 times the diameter of the propeller, i.e., 175 mm. In a free-field model, the sources are in unbounded water and radiated sound field is recovered on a hemispherical data recovery mesh having radius of 2 m.

Other arrangements than monopole rings, such as dipole rings, were tested. No clear added value compared to the simpler arrangement used was seen. When using dipoles, also the dipole axis, with length and orientation, needs to be defined. This information is not easy to define for a propeller and its blades using an "engineering judgement". Thus, applying dipoles lead easily to unnecessary complexity of equivalent source array selection.

Also, a very simple model, consisting of one monopole source in the exact centre of the tunnel was tested. The results concerning overall sound power as well as low-frequency sound pressure levels were decent. However, large (over 25 dB) point-wise sound pressure level errors occurred above 800 Hz. This is a demonstration of the sensitivity of high-frequency sound pressure to the location of a single source in an acoustic waveguide. A single monopole source is not able to reproduce the intricacy of sound field at high frequencies.

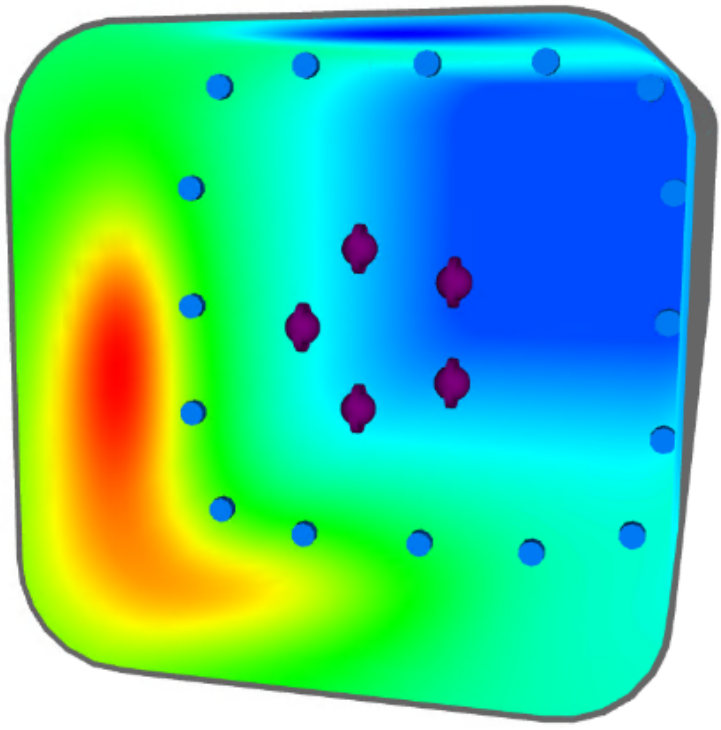

Figure 8. The 5-monopole equivalent source arrangement and 16 pressure sensors in the BEM-model. The sensor array of 16 sensors is placed 200 mm downstream from the source ring. The sensors are at 25 mm distance from the tunnel wall.

As explained above, the conditioning is represented by the condition number, which is shown in Figure 9 for the 5-monopole-16-sensor model.

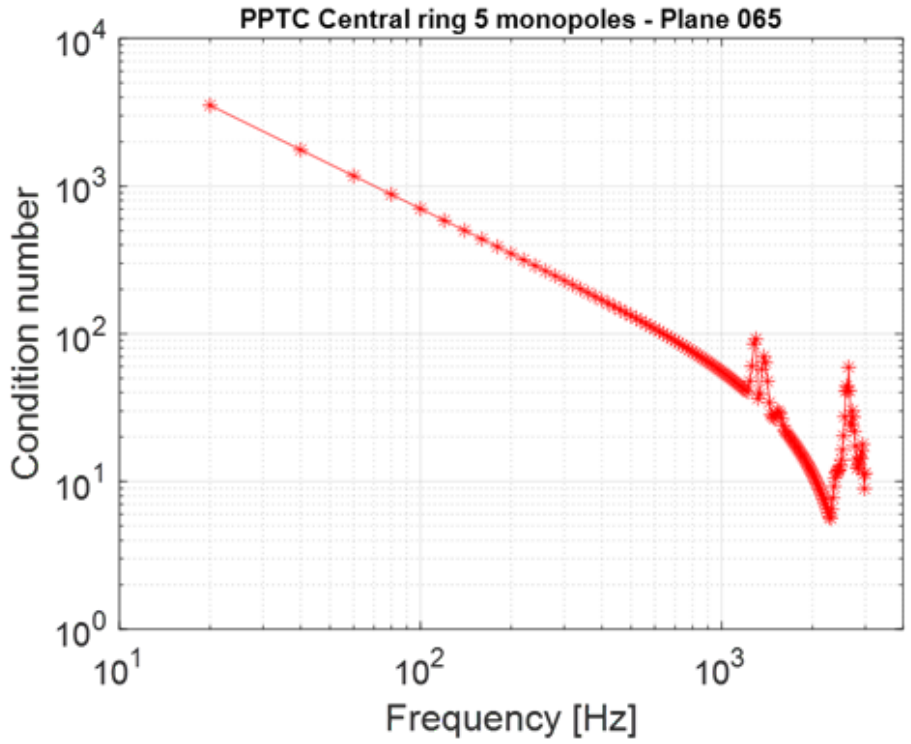

Figure 9. Condition number for the 5-monopole-16-sensor model transfer matrix H or H^+.

According to results of Figure 9, the matrix equations should be well-behaving except at the lowest frequencies below 60 Hz.

After calculation of the transfer matrix, the performance of the model in inverse source characterization was tested with given source vector. The frequency range was 20 to 3000 Hz with 20 Hz step. The test source volume velocity magnitudes and phases were as in Table 1.

Table 1. Source parameters of the test model.

Monopole Number	Magnitude of Q [m^3/s]	Phase of Q [Radians]
1	1	0
2	0.01	$\pi/4$
3	0.5	$\pi/3$
4	0.05	$\pi/2$
5	0.2	π

The results are in Figure 10. The given source vector was determined with high accuracy. Maximum relative error of magnitude was approx. 0.5 % (0.04 dB) whereas the maximum absolute error of the phase was approx. 0.2 degrees (0.003 radians). Hence, the model passed the test and was judged to be admissible for further use.

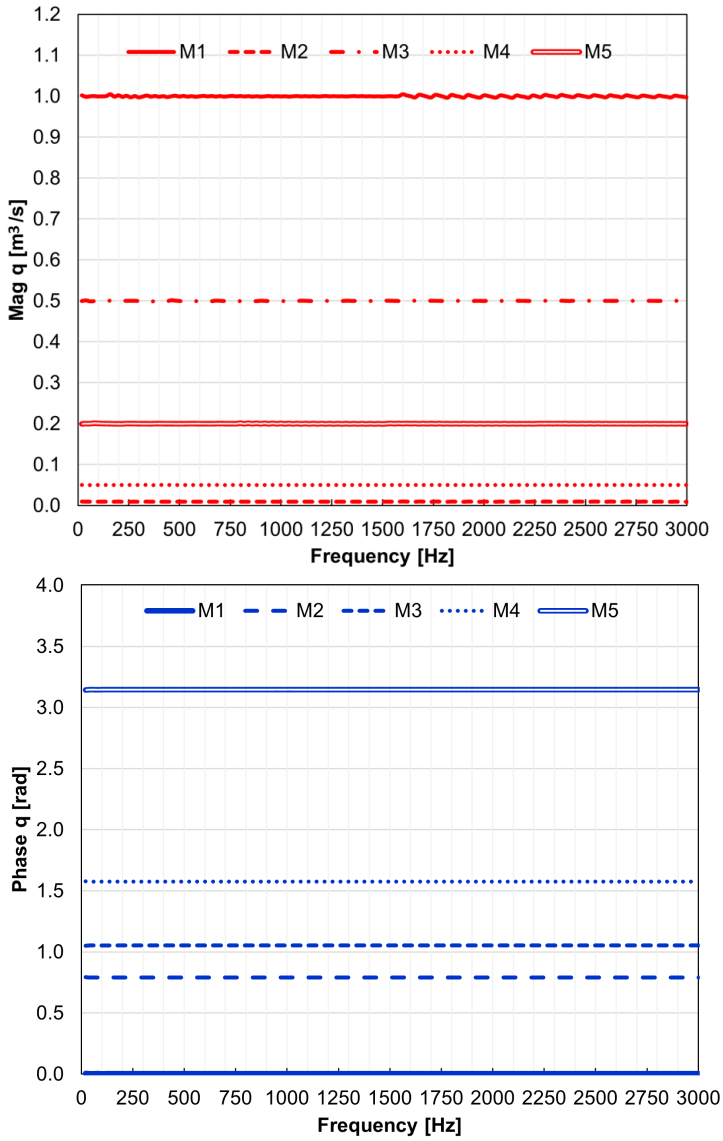

Figure 10. Results of the inverse TEST model with known sources. Magnitude (**top**), phase (**bottom**).

6. Discussion

Field point sound pressures calculated with FEM were used for the corresponding source vector according to Equation (6). After the source vector was calculated, the field sound pressure vector as well as tunnel-radiated sound power level were calculated using the BEM-model. Finally, the equivalent source model was transferred to free field and sound power levels were calculated.

Sound power of the PPTC in cavitation tunnel due to surface excitations from the complete simulation model and from the equivalent source model are compared in Figure 11. In Figure 12, the corresponding sound powers in free field are compared. As can be noted from Figure 11, the sound powers are similar meaning that the inverse source fitting of the excitations is fairly accurate. From Figure 12 it is notable that the equivalent excitations yields to similar net effect as the original ones, i.e., the source fit model is fairly independent from surroundings. These results show, that the propeller source was successfully decoupled from the reverberant tunnel environment and transferred to a completely different acoustic environment, free field in unbounded fluid. This opens up new opportunities in ship underwater noise simulations, because the propulsor as a sound source and its sound radiation need not to be tied to certain acoustic environment and pressure responses detected in that environment.

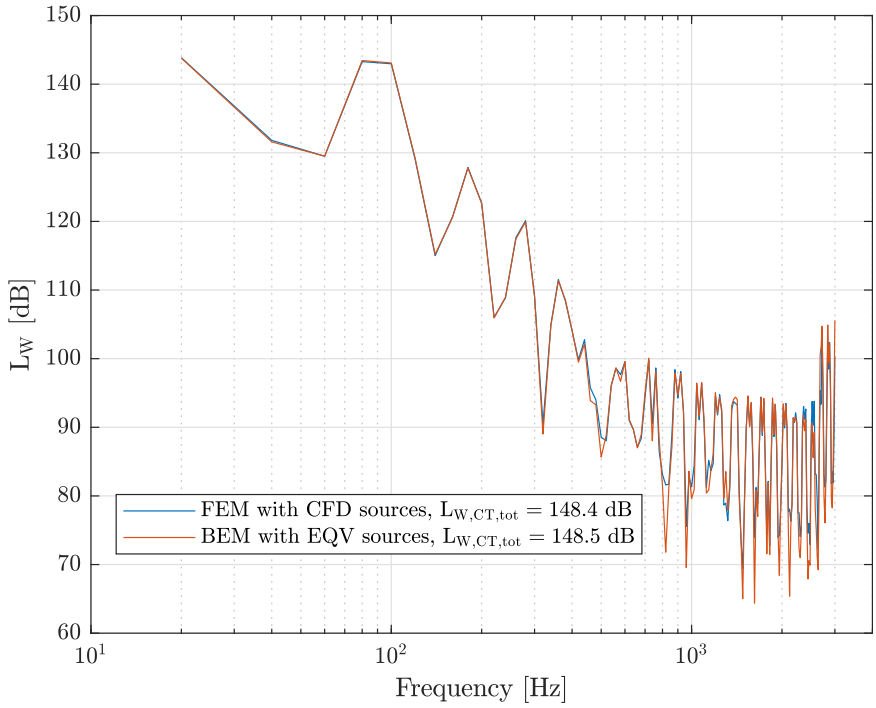

Figure 11. Sound powers in a cavitation tunnel from the complete simulation model and from the model with equivalent sources from inverse source fit.

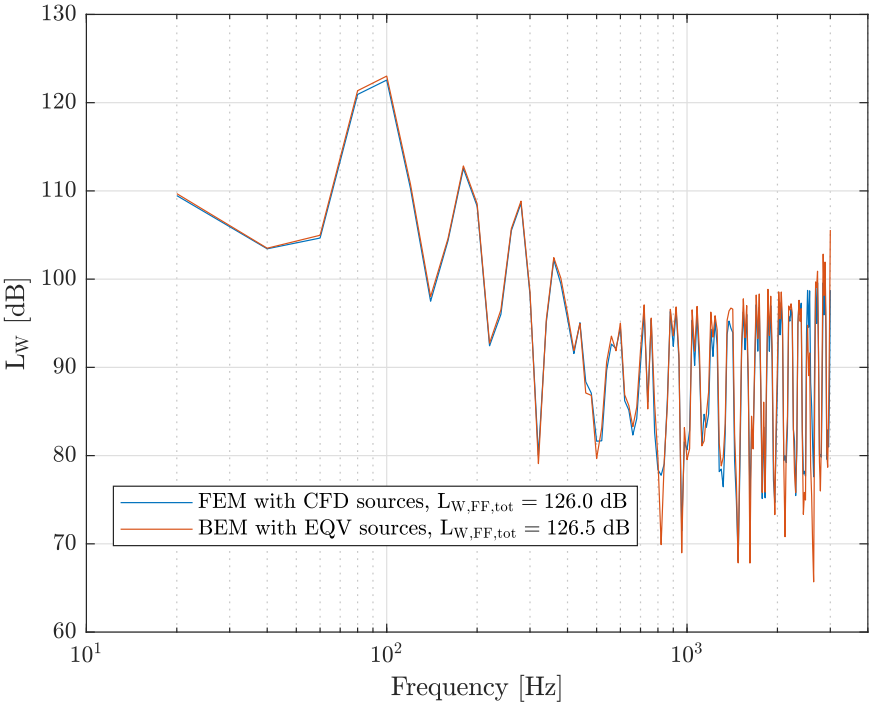

Figure 12. Sound powers in free field from the complete simulation model and from the model with equivalent sources from inverse source fit.

7. Conclusions

The introduced acoustic source characterization procedure of marine propulsors is applicable also for the responses determined experimentally in a cavitation tunnel when the pressure transducer array is determined appropriately.

The influence of the turbulence and vortices in the wake field, i.e., Lighthill's volume sources, will be investigated in the future. Other future work involves modelling of full-scale propulsors in natural environment including water-air or water-ice interface and the effects of ship hull reflection and elasticity. Also, the use of equivalent source models in digital twins via hull pressure monitoring, pre-defined substitute sources and pre-computed transfer matrices provides new possibilities in real-time in-situ estimation of ship URN and sound fields.

Author Contributions: A.H. conducted the acoustic FEM simulations and analyses with the complete model. J.T. conducted the inverse source fit and conducted the acoustic BEM simulations and analyses with the equivalent source model. All authors have read and agreed to the published version of the manuscript.

Funding: This research was funded by VTT Technical Research Centre of Finland Ltd. and Business Finland as part of UltraPropulsor project.

Institutional Review Board Statement: Not applicable.

Informed Consent Statement: Not applicable.

Data Availability Statement: Not applicable.

Conflicts of Interest: The authors declare no conflict of interest.

Abbreviations

The following abbreviations are used in this manuscript:

BEM	Boundary Element Method
BPF	Blade Passing Frequency
CFD	Computational Fluid Dynamics
CHA	Computational Hydro-acoustics
DNS	Direct Numerical Simulation
FEM	Finite Element Method
PPTC	Potsdam Propeller Test Case
SVD	Singular Value Decomposition
URN	Underwater Radiated Noise

References

1. Directive, Strategy Framework. Directive 2008/56/EC of the European Parliament and of the Council. Council Decision of 2008. Available online: https://www.legislation.gov.uk/eudr/2008/56/contents (accessed on 5 September 2022).
2. van der Graaf, A.J.; Ainslie, M.A.; André, M.; Brensing, K.; Dalen, J.; Dekeling, R.P.A.; Robinson, S.P.; Tasker, M.L.; Thomsen, F.; Werner, S. *European Marine Strategy Framework Directive Good Environmental Status (MSFD-GES). Report of the Technical Subgroup on Underwater Noise and Other Forms of Energy*; TSG Noise & Milieu Ltd.: Brussels, Belgium, 2012; pp. 1–75.
3. Mitson, R.B. (Ed.) *Underwater Noise of Research Vessels. Review and Recommendations*; Cooperative Research Report No. 209 (Issue 209); ICES: Copenhagen, Denmark, 1995.
4. Colbert, B.R. Trends and developments in international regulation of anthropogenic sound in aquatic habitats. *J. Acoust. Soc. Am.* **2020**, *147*, 3100–3107. [CrossRef] [PubMed]
5. ABS. Underwater Noise. In *Guide for Classification Notation*; American Bureau of Shipping: Houston, TX, USA, 2018; p. 32.
6. Bureau Veritas. Underwater Radiated Noise (URN). Rule Note 2014, NR 614 DT R00 E, 33(614). Marine & Offshore 92937 Paris la Défense Cedex—France. Available online: https://ec.europa.eu/environment/marine/pdf/MSFD_reportTSG_Noise.pdf (accessed on 5 September 2022).
7. DNV. Chapter 24—Silent Class Notation. In *Det Norske Veritas, Rules for Classification of Ships–Newbuildings*; DNV: Bærum, Norway, 2010; p. 18.
8. IMO. *Guidelines for the Reduction of Underwater Noise from Commercial Shipping to Address Adverse Impacts on Marine Life*; International Maritime Organization: London, UK, 2014.
9. Arveson, P.T.; Vendittis, D.J. Radiated noise characteristics of a modern cargo ship. *J. Acoust. Soc. Am.* **2000**, *107*, 118–129. [CrossRef] [PubMed]
10. Bark, G.; van Berlekom, W.B. Experimental investigations of cavitation dynamics and cavitation noise. In Proceedings of the Twelfth Symposium of Naval Hydrodynamics, Washington, DC, USA, 9–14 August 1979; National Academy of Sciences: Washington, DC, USA, 1979; pp. 470–493.

11. Doolan, C.; Brandner, P.; Butler, D.; Pearce, B.; Moreau, D.; Brooks, L. Hydroacoustic characterisation of the amc cavitation tunnel. In Proceedings of the Acoustics 2013 Victor Harbor: Science, Technology and Amenity, Victor Harbor, Australia, 17–20 November 2013.
12. Felli, M. Noise measurements techniques and hydrodynamic aspects related to cavitation noise. In *HydroTesting Alliance (HTA), an Alliance to Enhance the Maritime Testing Infrastucture in the EU 2011*; Project No.: 031316, Sixth Framework Programme Priority 1.6.2; Sustainable Surface Transport: Brussels, Belgium, 2011. Available online: https://core.ac.uk/download/pdf/37833561.pdf (accessed on 5 September 2022).
13. Jeona, J.-H.; Joob, W.-H.P. Prediction of propeller radiated noise by onboard measurement. In Proceedings of the 2nd International Conference and Exhibition on Underwater Acoustics, Rhodes, Greece, 22–27 July 2014; pp. 667–674.
14. Tani, G.; Viviani, M.; Hallander, J.; Johansson, T.; Rizzuto, E. Propeller underwater radiated noise: A comparison between model scale measurements in two different facilities and full scale measurements. *Appl. Ocean Res.* **2016**, *56*, 48–66. [CrossRef]
15. Tani, G.; Viviani, M.; Felli, M.; Lafeber, F.H.; Lloyd, T.; Aktas, B.; Atlar, M.; Turkmen, S.; Seol, H.; Hallander, J.; et al. Noise measurements of a cavitating propeller in different facilities: Results of the round robin test programme. *Ocean Eng.* **2020**, *213*, 107599. [CrossRef]
16. Viitanen, V.M.; Hynninen, A.; Tanttari, J.; Sipilä, T.; Lübke, L.; Klose, R.; Siikonen, T. CFD and CHA simulation of the underwater noise induced by a marine propeller in two-phase flows. In Proceedings of the Fifth International Symposium on Marine Propulsors Smp'17, Espoo, Finland, 12–15 June 2017.
17. Viitanen, V.M.; Hynninen, A.; Sipilä, T.; Siikonen, T. DDES of Wetted and Cavitating Marine Propeller for CHA Underwater Noise Assessment. *J. Mar. Sci. Eng.* **2018**, *6*, 56. [CrossRef]
18. Tadros, M.; Ventura, M.; Guedes Soares, C. Design of Propeller Series Optimizing Fuel Consumption and Propeller Efficiency. *J. Mar. Sci. Eng.* **2021**, *9*, 1226. [CrossRef]
19. Uosukainen, S. *Foundations of Acoustic Analogies*; VTT Publications 757; VTT Technical Research Centre of Finland: Espoo, Finland, 2011.
20. Mohsen, G.; Hassan, G.; Jalal, M. Calculation of sound pressure level of marine propeller in low frequency. *J. Low Freq. Noise Vib. Act. Control* **2018**, *37*, 60–73. [CrossRef]
21. Lidtke, A.K.; Turnock, S.R.; Humphrey, V.F. Characterisation of sheet cavity noise of a hydrofoil using the Ffowcs Williams–Hawkings acoustic analogy. *Comput. Fluids* **2016**, *130*, 8–23. [CrossRef]
22. Lidtke, A.K.; Lloyd, T.; Lafeber, F.H. Predicting cavitating propeller noise in offdesign conditions using scale-resolving CFD simulations. *Ocean Eng.* **2022**, *254*, 111176. [CrossRef]
23. Nelson, P.A.; Yoon, S.H. Estimation of acoustic source strength by inverse methods: Part I, conditioning of the inverse problem. *J. Sound Vib.* **2000**, *2330*, 639–664. [CrossRef]
24. Yoon, S.H.; Nelson, P.A. Estimation of acoustic source strength by inverse methods: Part II, experimental investigation of methods for choosing regularization parameters. *J. Sound Vib.* **2000**, *233*, 665–701. [CrossRef]
25. Kim, Y.; Nelson, P.A. Estimation of acoustic source strength within a cylindrical duct by inverse methods. *J. Sound Vib.* **2004**, *275*, 391–413. [CrossRef]
26. Moorhouse, A.T.; Seiffert, G. Characterisation of an airborne sound source for use in a virtual acoustic prototype. *J. Sound Vib.* **2006**, 296, 334–352. [CrossRef]
27. Berckmans, D.; Kindt, P.; Sas, P.; Desmet, W. Evaluation of substitution mono-pole models for tire noise sound synthesis. *Mech. Syst. Signal Process.* **2010**, *24*, 240–255. [CrossRef]
28. Lee, K.; Lee, J.; Kim, D.; Kim, K.; Seong, W. Propeller sheet cavitation noise source modeling and inversion. *J. Sound Vib.* **2014**, *333*, 1356–1368. [CrossRef]
29. Kim, D.; Lee, K.; Seong, W. Non-cavitating propeller noise modeling and inversion. *J. Sound Vib.* **2014**, *333*, 6424–6437. [CrossRef]
30. Lee, S. Review: The Use of Equivalent Source Method in Computational Acoustics. *J. Comput. Acoust.* **2017**, *25*, 1630001. [CrossRef]
31. Virovlyansky, A.L.; Deryabin, M.S. On the use of the equivalent source method for free-field calibration of an acoustic radiator in a reverberant tank. *J. Sound Vib.* **2019**, *455*, 69–81. [CrossRef]
32. Chu, N.; Huang, Q.; Yu, L.; Ning, Y.; Wu, D. Rotating acoustic source localization: A power propagation forward model and its high-resolution inverse methods. *Meas. J. Int. Meas. Confed.* **2021**, *174*, 109006. [CrossRef]
33. Ochmann, M.; Piscoya, R. *Theory and Application of Acoustic Sources Using Complex Analysis*; Springer: Berlin/Heidelberg, Germany, 2021. [CrossRef]
34. Zhang, L.; Wang, J.; Yang, D.; Hu, B.; Wu, D. Optimization of the equivalent source configuration for the equivalent source method. *J. Mar. Sci. Eng.* **2021**, *9*, 807. [CrossRef]
35. Palleja-Cabre, S.; Tester, B.J.; Astley, R.J. Modelling of ducted noise sources in the proximity of acoustic liners. *J. Sound Vib.* **2021**, *517*, 116548. [CrossRef]
36. Hynninen, A.; Tanttari, J.; Viitanen, V.M.; Sipilä, T. On predicting the sound from a cavitating marine propeller in a tunnel. In Proceedings of the Fifth International Symposium on Marine Propulsors Smp'17, Espoo, Finland, 12–15 June 2017.
37. Pierce, A.D. Acoustics: An introduction to its physical principles and applications. In *Acoustical Society of America*; Springer: Berlin/Heidelberg, Germany, 1989.

38. Russell, D.A.; Titlow, J.P.; Bemmen, Y.-J. Acoustic monopoles, dipoles, and quadrupoles: An experiment revisited. *Am. J. Phys.* **1999**, *67*, 660–664. [CrossRef]
39. Barkmann, U.; Heinke, H.-J.; Lübke, L. Potsdam Propeller Test Case (PPTC). In Proceedings of the Second International Symposium on Marine Propulsors Smp'11, Hamburg, Germany, 15–17 June 2011; pp. 36–38.
40. SVA. Potsdam Propeller Test Case PPTC. Available online: https://www.sva-potsdam.de/en/potsdam-propeller-test-case-pptc/ (accessed on 1 August 2022).
41. Klose, R. *Noise Measurements with the Model Propellers P1790 (PPTC) and P1806 (High Efficiency Propeller) in Homogeneous Inflow*; Report 4589; Schiffbau Versuchsanstalt Potsdam: Potsdam, Germany , 2018.